PCCP

PAPER

Cite this: *Phys. Chem. Chem. Phys.*, 2015, **17**, 4441

Liquid crystal seed nucleates liquid–solid phase change in ceria nanoparticles

Thi X. T. Sayle, Lewis W. L. Sayle and Dean C. Sayle*

Received 26th November 2014,
Accepted 31st December 2014

DOI: 10.1039/c4cp05499g

www.rsc.org/pccp

Molecular dynamics (MD) simulation was used to explore the liquid–solid (crystal) phase change of a ceria nanoparticle. The simulations reveal that the crystalline seed, which spontaneously evolves and nucleates crystallisation, is a liquid rather than a solid. Evidence supporting this concept includes: (a) only 3% of the total latent heat of solidification had been liberated after 25% of the nanoparticle had (visibly) crystallised. (b) Cerium ions, comprising the (liquid) crystal seed had the same mobility as cerium ions comprising the amorphous regions. (c) Cerium ion mobility only started to reduce (indicative of solidification) after 25% of the nanoparticle had crystallised. (d) Calculated radial distribution functions (RDF) revealed no long-range structure when 25% of the nanoparticle had (visibly) crystallised. We present evidence that the concept of a liquid crystal seed is more general phenomenon rather than applicable only to nanoceria.

Introduction

Classical Nucleation Theory (CNT) describes the process underpinning a phase change from a liquid phase to a solid (crystal) phase[1] and is central to the evolution of a material microstructure, which governs its physical, chemical and mechanical properties. The microstructure includes, for example, the polymorphic crystal structure (polymorphic forms of carbon include graphite and diamond, which have very different properties); morphology and the surfaces exposed with implications for the catalytic activity;[2] dislocations and grain-boundaries, which impact upon the mechanical properties;[3] point defects, which are pivotal to electronic and ionic conductivity with application for solid oxide fuels[4] and catalysis.[5]

Understanding, at the atom level, of the mechanism underpinning crystallisation, whether from solution[6] or the freezing of a liquid,[7] has been the subject of intense scrutiny spanning many decades because such understanding will facilitate the ability to control the crystallisation and realise desirable microstructures for targeted application. Moreover, with the recent discovery of nanoparticle-mediated crystallization theory (non-classical crystallisation) the field remains the subject of intense scientific interest and scrutiny.[8]

Experimentally, it is very difficult to characterise, with atom-level resolution, the time resolved homogeneous crystallisation of a material *via* the spontaneous evolution of a crystalline nucleating seed,[9] and therefore computer simulation can provide unique insight.[10]

Atomistic simulation has been used to explore the freezing of water,[11] metals[12] and nanoparticles,[13] crystallisation from solution,[6] and biotemplated crystallisation.[14] However, a major obstacle with simulating crystallisation directly, using molecular dynamics (MD) simulation, are the high energy barriers associated with evolving a solid crystalline seed starting from an amorphous precursor. In particular, MD is only able to simulate small windows in time – typically of the order of nanoseconds, which reduces the probability of simulating the potential hypersurface sufficiently to capture the spontaneous evolution of the seed within the duration of the simulation. Accordingly, accelerated dynamics has been used to overcome such limitations.[14] However, as Anwar and Zahn report: 'you don't gain something for nothing' and the approximations of accelerating the dynamics means that certain choices with regards to the final state and pathway must be made, which can obscure alternative pathways that the system may take during the crystallisation process.[10]

Here, we use molecular dynamics simulation to explore directly the nucleation and crystal growth of ceria nanoparticles, which are widely exploited in applications spanning: catalysis[15] to nanomedicine.[16]

Methods

The calculations presented in this study are based upon the Born model of the ionic solid, where the energy of the system is given by:

$$E(r_{ij}) = \sum_{ij} \frac{Q_i Q_j}{4\pi\varepsilon_o r_{ij}} + \sum_{ij} A \exp\left(\frac{-r_{ij}}{\rho}\right) - C r_{ij}^{-6},$$

the first term represents the Coulombic interaction between ion i of charge Q_i and ion j of charge Q_j, which are a distance r_{ij} apart. The second term is of the Buckingham form, which is

School of Physical Sciences, University of Kent, Canterbury, CT2 7NZ, UK. E-mail: d.c.sayle@kent.ac.uk

particularly effective in representing ionic solids. Model parameters, used to describe CeO_2 and water together with the interactions between ceria and water were taken from ref. 17. The molecular dynamical simulations were performed using the DLPOLY code.[18]

To simulate solidification, a nanoparticle of ceria was first melted by heating it at a temperature above its melting point and then solidified by cooling the nanoparticle at a temperature below its melting point using MD simulation; analysis of the dynamical trajectories of the ions, using analytical and molecular graphical techniques, was then used to elucidate the mechanisms underpinning the solidification process.

Specifically, a cube of ceria comprising 15 972 atoms was cleaved from the parent bulk material and melted by performing MD simulation at 6500 K using a 0.001 ps time-step. After 14 000 cycles of MD simulation (14 ps) the nanoparticle was observed to be liquid phase. The model nanoparticle was then immersed in water and the temperature was reduced to 2390 K. MD simulation was performed for 2500 ps using a 0.003 ps time-step, during which time the nanoparticle solidified.

The MD simulations were performed using an *NPT* ensemble (constant number of particles, constant pressure, constant temperature). The pressure was set to zero with thermostat and barostat relaxation times of 0.1 and 0.5 ps respectively; a real-space potential cut-off of 10.0 Å and an Ewald precision of 10^{-6} was employed.

We note that the water molecules were held fixed during the crystallisation, which is unphysical. However, the reason for immersing the nanoparticle in water was not to simulate the influence of an aqueous environment on the solidification; rather it was to ensure that the nanoparticle did not rotate during the solidification. If the nanoparticle is allowed to solidify in vacuum, the latent heat of solidification can sometimes be converted into rotational energy. Such rotation of the nanoparticle would prevent reliable extraction of the individual atom velocities from the simulation because the velocities of the ions would include a contribution from the rotational velocity. The role of the water was therefore wholly to provide a cavity in which the nanoparticle can solidify without rotating. The system pressure during the simulation was calculated to be 0 ± 0.05 kbar and therefore the cavity does not constrain the nanoparticle to crystallise under (high) pressure.

The chosen temperature (2390 K) is critical to the simulation of the solidification. In particular, preliminary simulations revealed that at 2800 K the nanoparticle was molten but as the temperature was reduced to 2600 K the nanoparticle crystallised. The melting point of the nanoparticle (associated with the potential model) therefore lies between 2600 and 2800 K. Preliminary simulations revealed that the speed of crystallisation increases with increasing temperature. We propose that at 2600 K the crystallisation speed is higher compared to crystallisation at a lower temperature because at the higher temperature there is a higher probability that individual ions have sufficient energy to overcome the barriers associated with locating to lattice sites to propagate the crystallisation (exploring configurational space). Conversely, a fast speed of crystallisation reduces the size of the trajectory data, which emanates from the MD simulation; the trajectory data comprises the positions, velocities and accelerations of the ions as a function of time. Accordingly, to better 'observe' and understand the solidification, a (supercooled) temperature of 2390 K was chosen, which reduced the speed of the crystallisation, increased the size of the trajectory data and hence increased the amount of mechanistic detail that could be extracted from the trajectory data (albeit at increased computational cost); the simulation required about 50 000 cpu hours.

Results

In this section, we analyse the trajectory data using analytical and molecular graphical techniques to: characterise the atomistic structure of the nanoparticle as it crystallises; calculate the heat of solidification emanating from the nanoparticle; characterise the atomistic structure of the nanoparticle during the embryonic stages of solidification; calculate the mobility of the cerium cations and oxygen anions during solidification; determine the long-range structural order of the nanoparticle during solidification and elucidate the mechanisms associated with the propagation of crystallisation – emanating from the nucleating seed.

Crystallisation

The configuration energy, average cerium ion velocity and structure of the CeO_2 nanoparticle, calculated as a function of time, are shown in Fig. 1. The figure reveals that the nanoparticle is initially liquid, Fig. 1(b), and then at a particular instance in time a crystalline seed *spontaneously* evolves within the amorphous sea of ions, Fig. 1(c). The seed then grows in size, Fig. 1(d–f) until the whole nanoparticle is crystalline, Fig. 1(g).

Latent heat of solidification

During the whole simulation, the configurational energy decreases by 180 kJ kg^{-1}, which reflects the latent heat of solidification. At 675 ps, about 25% of the nanoparticle is observed to be crystalline, Fig. 1(e). Accordingly, one might expect that the decrease in configurational energy at 675 ps would be 45 kJ kg^{-1} or 25% of the total latent heat. However, the decrease in configurational energy at this point is only 6 kJ kg^{-1} or 3% of the total latent heat of solidification. This suggests that the crystalline seed may not exist as a solid.

Embryonic stages of solidification

In fluorite-structured CeO_2, the energy barriers associated with Ce mobility are so high that Ce mobility within the lattice cannot be 'observed' using MD simulation. Accordingly, we used this criterion to determine the phase (liquid or solid) of the CeO_2. In particular, all Ce ions that are mobile during the MD simulation are deemed to be liquid phase. Specifically, the criterion for determining Ce mobility was to identify Ce ions, which escape their lattice site and move further than the nearest interstitial position. In fluorite-structured CeO_2 nanoparticle, the distance from a cerium lattice point to the nearest interstitial site is 1.35 Å. If the material were a crystalline solid,

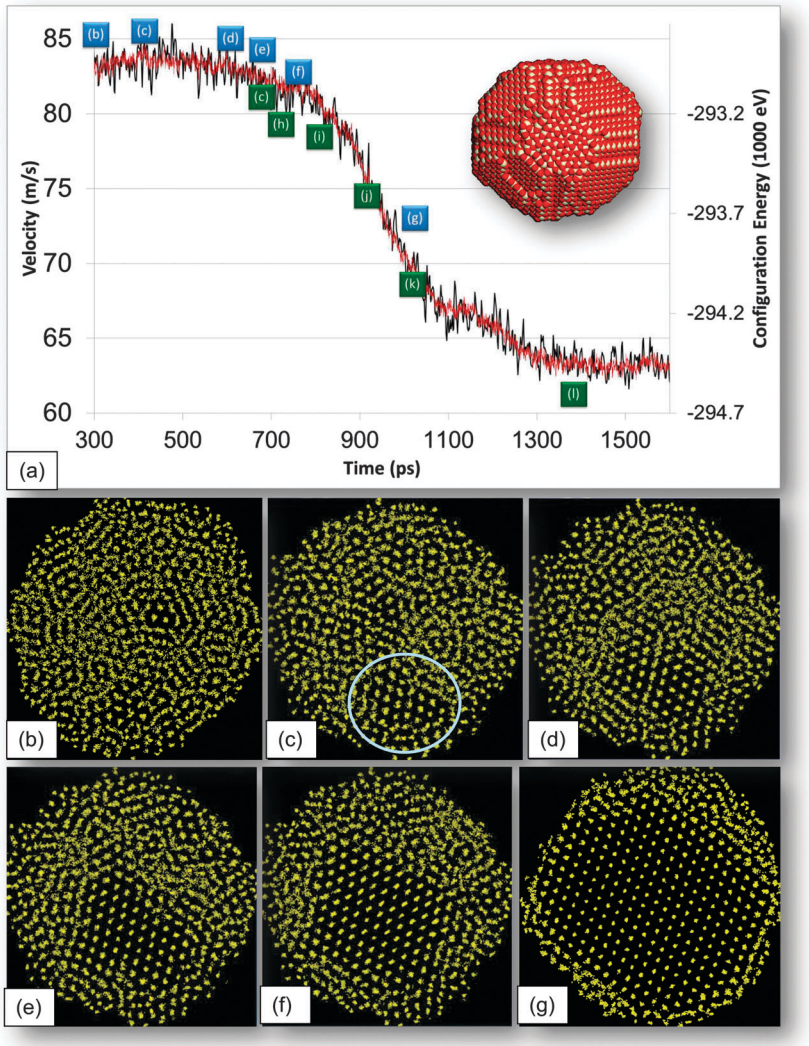

Fig. 1 (a) Average Ce ion velocity (red trace, first ordinate), configurational energy (black trace, second ordinate) of the CeO_2 nanoparticle, calculated as a function of time. Ce atom positions (yellow) comprising the nanoparticle, at selected times during the crystallisation, are shown in: (b) 300 ps, (c) 415 ps, (d) 600 ps, (e) 675 ps, (f) 750 ps, (g) 1000 ps. The configurational energy of each structure is annotated (blue labels) in (a). The fully crystallised CeO_2 nanoparticle is shown top right in (a); cerium is coloured white and oxygen is red. Green labels in (a) correlate to the solidification, Fig. 2.

the Ce ions would not be observed to escape their lattice sites and move past the nearest interstitial site under MD simulation because of the high associated energy barrier. Accordingly, to determine the onset of solidification, those cerium ions, which moved less than 1.5 Å during a 75 ps interval, were identified as ions comprising solid regions of the nanoparticle. The strategy enabled the spontaneous evolution, embryonic structure and growth of the *solid* phase to be mapped, Fig. 2, and can be usefully correlated with the configurational energy, Fig. 1(a); (green labels).

The structures, shown in Fig. 2, reveal that the onset of solidification occurs at about 665 ps – no ions were identified to have mobilities of less than 1.5 Å/75 ps before this time. At 675 ps, the fluorite structure becomes evident, Fig. 2(c). However, the size of the solid region at 675 ps, Fig. 2(c), is much smaller than the crystalline region, Fig. 1(e), at 675 ps. Indeed, a crystalline seed is visible as early as 415 ps, Fig. 1(c), which is much earlier than the onset of solidification (665 ps). The simulations therefore reveal that the crystalline seed, Fig. 1(c) and (d), is liquid. Moreover, analysis of the MD trajectory confirmed that the cations comprising the crystalline seed are able to diffuse and move between lattice sites.

Ionic mobility

Cerium and oxygen Mean square displacements (MSD), calculated as a function of time, are shown in Fig. 3. The onset of crystallisation (at 415 ps, Fig. 1(c)) and the onset of solidification (665 ps, Fig. 2(a)) are indicated on the figure using dashed lines. The gradient of the MSD trace, which reflects the ionic mobility, remains constant from before the onset of crystallisation up to about 700 ps at which point over 25% of the nanoparticle is crystalline, Fig. 1(e) and (f). Accordingly, the mobility of ions comprising the

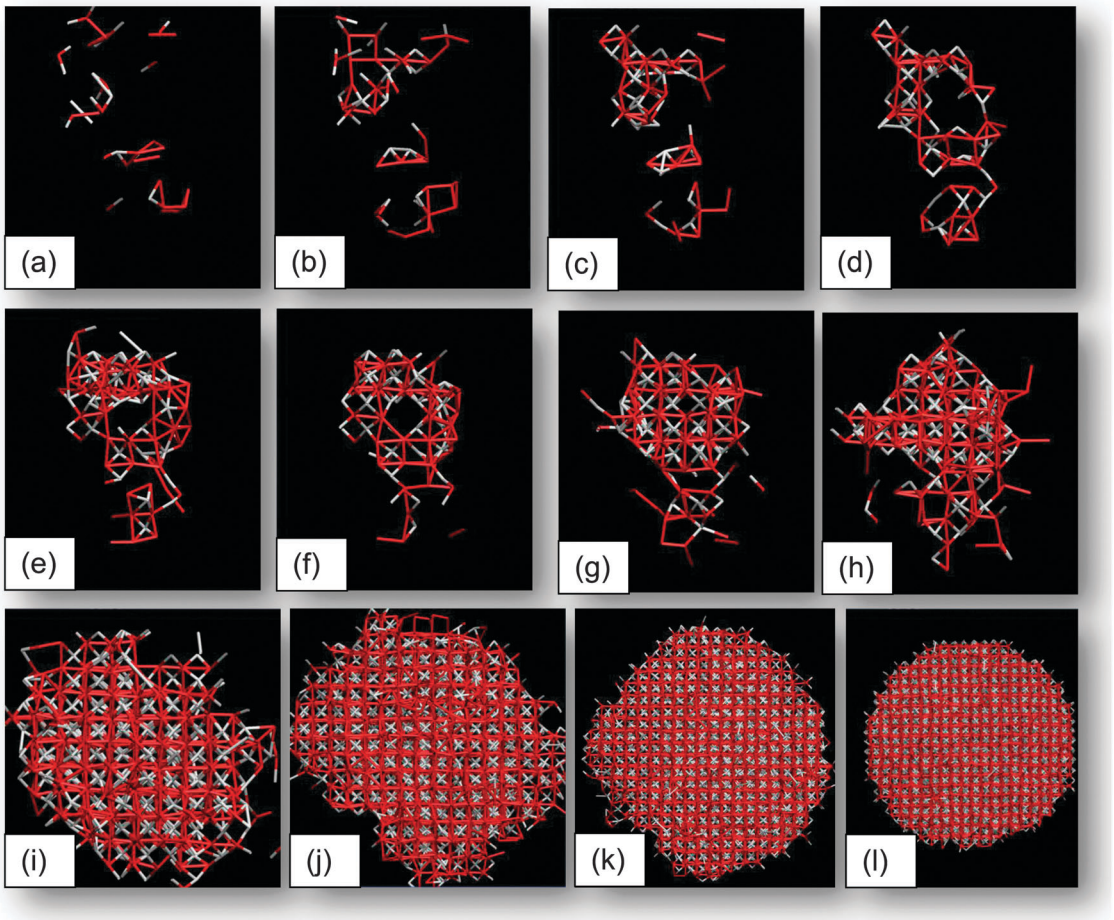

Fig. 2 Spontaneous evolution, growth and embryonic structure of the solid crystalline seed as a function of time. (a) 665 ps (b) 670 ps (c) 675 ps (d) 680 ps (e) 685 ps (f) 690 ps (g) 700 ps (h) 710 ps (i) 800 ps (j) 910 ps (k) 1000 ps (l) 1350 ps. Ce ions are coloured white and oxygen is red. The configurational energies of the structures are indicated, green labels, in Fig. 1(a).

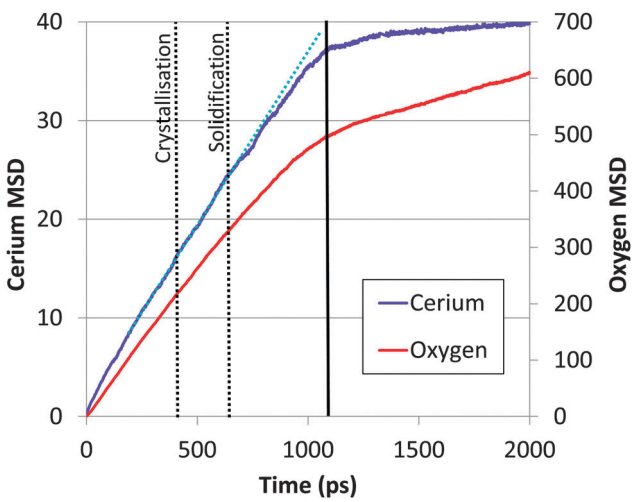

Fig. 3 Mean Square Displacements (Å^2) calculated as a function of time (ps). The light blue dashed line, superimposed over the cerium ion MSD trace, shows that the mobility of the cerium ions does not change during the period of time in which over 25% of the nanoparticle crystallises.

crystalline region is commensurate with the mobility of ions comprising the amorphous regions because if the mobility of ions comprising the crystalline regions reduced, this would be reflected in a reduction in the gradient of the MSD trace. After 700 ps, the MSD trace exhibits a reduction in the gradient indicating a reduction in the average cation mobility.

At about 1100 ps, the gradient of the MDS trace, Fig. 3, shows a sharp discontinuity and indicates that the nanoparticle is entirely solid. We note that the gradient of the MSD trace above 1100 ps is not zero; analysis of the cerium ion mobility, using molecular graphics, reveals that the residual mobility is attributed to Cerium ions moving on the surface of the nanoparticle.

Nanoparticle crystallinity

To further identify the onset of solidification, the Ce–Ce, Ce–O and O–O radial distribution functions (RDF) were calculated as a function of time. The RDF traces revealed evidence of the onset of long-range order (indicative of crystallinity) of the nanoparticle at about 900 ps. In particular, Fig. 4 shows the next-nearest-neighbour Ce–Ce peak starting to emerge at 900 ps. Prior to this time, the RDF traces are broad and commensurate with an amorphous (molten)

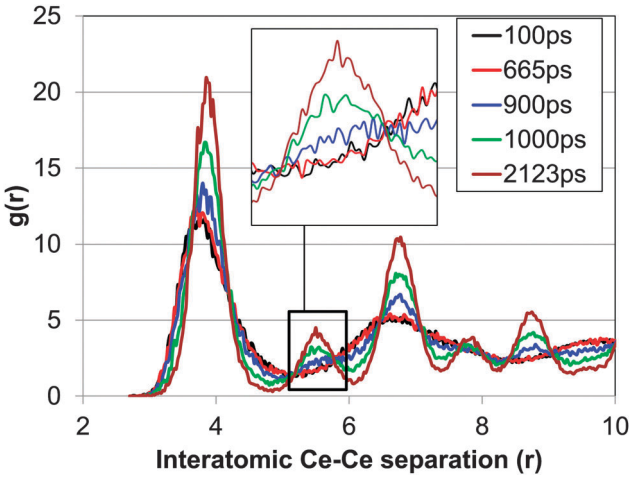

Fig. 4 Ce–Ce Radial Distribution Functions, calculated as a function of time during the crystallisation and solidification of the ceria nanoparticle. Interatomic separations are shown in Å.

structure. Conversely, 25% of the nanoparticle is (visually) crystalline at 675 ps, Fig. 1(e). We attribute this anomaly, between the analytical appraisal of the crystallinity (*via* RDF) compared to the visual appraisal of the crystallinity, to the disorder of the crystalline seed. In particular, visually the ions appear to be located at lattice sites, but careful inspection reveals that the ions are somewhat disordered – analogous to a large thermal ellipsoid associated with each lattice site. Such disorder manifests within the RDF at the next-nearest-neighbour peak and beyond and therefore the long-range structure of the crystalline seed cannot be resolved within the RDF because of the thermal ellipsoids.

Propagation of crystallisation

The structure of the nanoparticle at 975 ps, Fig. 5(a), shows that almost all the cerium ions are ordered and located on (near) crystallographic lattice sites. However, in a shell comprising the nanoparticle, the oxygen ions are disordered (liquid-like), Fig. 5(b). The simulations reveal that crystallisation proceeds with the cations locating first to lattice sites and then the anions move to their respective lattice sites. Such crystallisation mechanisms are the same for all time periods in that as the crystallisation front emanates radially from the seed, the cerium sublattice crystallises first, followed by the oxygen ions. In particular, the ions 'pre-order' in the liquid phase and then solidify in this ordered state.

During crystallisation, point defects – including oxygen and cerium vacancies – evolve as a consequence of ions failing to occupy all available lattice sites. During the simulation, the oxygen vacancies are subsequently annealed out of the structure. In particular, the oxygen ions move, *via* a vacancy mechanism, to fill vacant positions. The mobility is concerted, with many oxygen ions moving at the same time. The pathways for the moving oxygen ions, together with the concerted movement can be seen in Fig. 6. Most diffusion pathways are along ⟨100⟩. However, there are a few jumps that occur along ⟨110⟩; the latter is highlighted in the circle in Fig. 6(b). Conversely, once solid, the cerium ions are unable to move under MD simulation and the cerium vacancies become trapped within the (model) structure.

The final, low temperature, structure of the CeO_2 nanoparticle (inset Fig. 1(a)) conforms to the fluorite crystal structure and comprises a polyhedral morphology with {111} surfaces truncated by {100} in accord with experiment.[13]

Discussion

The evidence that supports the concept that the crystalline seed, which nucleates the liquid–solid phase change, evolves as a liquid (crystal) rather than a solid (crystal) includes:

- (Only) 3% of the total calculated latent heat of solidification is liberated after 25% of the nanoparticle has crystallised, Fig. 1.
- Cerium ions, comprising the (liquid) crystal seed, have the same mobility as cerium ions comprising the amorphous regions, Fig. 3.
- Cation mobility starts to reduce after 25% of the nanoparticle is crystalline, Fig. 3.
- Calculated RDF's reveal no long-range structure within the nanoparticle when 25% of the nanoparticle is (visibly) crystalline, Fig. 4.

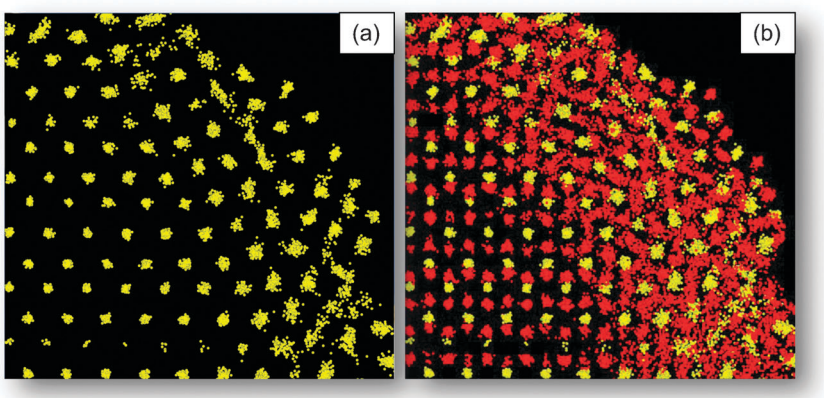

Fig. 5 Atom positions comprising the ceria nanoparticle at 975 ps. (a) Only cerium sublattice positions shown, (b) cerium and oxygen positions shown. Ce ions are coloured yellow and oxygen is red.

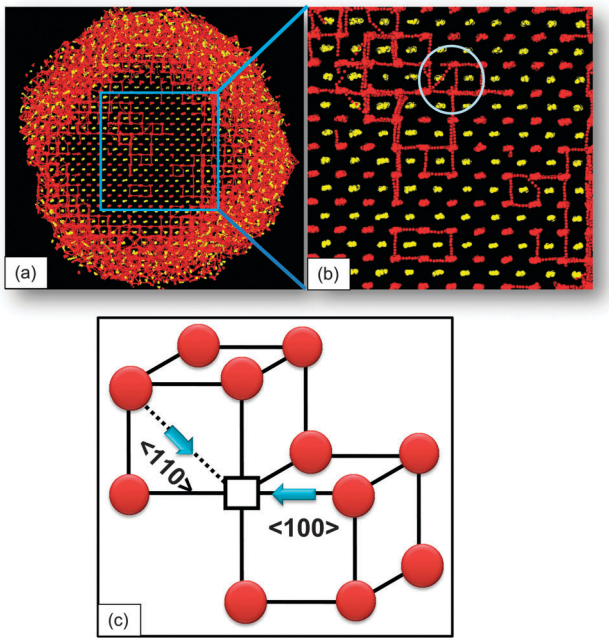

Fig. 6 Structure of the CeO_2 nanoparticle at 975 ps showing the oxygen diffusion mechanism. (a) Slice cut through the whole ceria nanoparticle. (b) Enlarged segment of (a) showing more clearly the diffusion pathways. (c) Schematic showing the diffusion pathways along ⟨100⟩ and ⟨110⟩ in the idealised fluorite structure. Cerium ion positions are coloured yellow and oxygen is red.

• Long-range structure starts to emanate (within the RDF) after more than 25% of the nanoparticle is crystalline, Fig. 2 and 4.

The spontaneous evolution of a crystalline seed, which nucleates a phase change from liquid to crystalline solid is a rare event because the energy barriers associated with ions rearranging from an amorphous to a crystalline solid are high. Accordingly, the structural hypersurface cannot be explored, within the timescales typically accessible to MD simulation, to facilitate spontaneous evolution of a crystalline seed. It is therefore surprising that such events have been documented in the open literature.[19] This can be explained if the crystalline seed spontaneously evolves as a *liquid* enabling MD simulation to adequately explore the potential hypersurface and spontaneously evolve a crystalline seed because the energy barriers for ion mobility in a liquid are normally much lower than for a solid. In particular, simulated crystallisation, using MD, has been used to 'observe' the crystallisation of water,[11] Li_2O (inverse fluorite),[20] TiO_2 (rutile),[21] ZnS (wurtzite),[19] MgO (rocksalt)[19] and MnO_2 (pyrolucite)[22] *via* the spontaneous evolution of a crystalline seed. Accordingly, we propose that nucleation of the liquid–solid phase change, *via* 'liquid' crystal seeds, is a more general phenomenon, applicable to other materials spanning several structural classes.

Conclusion

Molecular dynamics, which was used to simulate directly the crystallisation of a ceria nanoparticle, reveals that the mechanism associated with the liquid to solid (crystal) phase change is a two-step process. First, the amorphous liquid spontaneously evolves into a crystalline liquid, and then the crystalline solid emanates from within the liquid (crystal) phase. Propagation of crystallisation proceeds *via* the cations locating first to lattice sites surrounded by a sea of liquid oxygen ions; the oxygen anions then locate to their respective lattice sites.

Acknowledgements

EPSRC: EP/H001220/1.

References

1 D. Gebauer, M. Kellermeier, J. D. Gale, L. b. Lennart Bergstrom and H. Colfen, Pre-nucleation clusters as solute precursors in crystallisation, *Chem. Soc. Rev.*, 2014, **43**, 2348–2371.
2 Y. Li and W. Shen, Morphology-dependent nanocatalysts: Rod-shaped oxides, *Chem. Soc. Rev.*, 2014, **43**, 1543–1574.
3 T. Zhu. and J. Li, Ultra-strength materials, *Prog. Mater. Sci.*, 2010, **55**, 710–757.
4 L. Malavasi, C. A. J. Fisher and M. S. Islam, Oxide-ion and proton conducting electrolyte materials for clean energy, applications: structural and mechanistic features, *Chem. Soc. Rev.*, 2010, **39**, 4370–4387.
5 E. W. McFarland and H. Metiu, Catalysis by Doped Oxides, *Chem. Rev.*, 2013, **113**, 4391–4427.
6 S. Piana, M. Reyhani and J. D. Gale, Simulating micrometre-scale crystal growth from solution, *Nature*, 2005, **438**, 70–73.
7 Z. Materials and H. Stachurski, On Structure and Properties of Amorphous, *Materials*, 2011, **4**, 1564–1598.
8 R.-Q. Song, H. Colfen, A.-W. Xu, J. Hartmann and M. Antonietti, Polyelectrolyte-Directed Nanoparticle Aggregation: Systematic Morphogenesis of Calcium Carbonate by Nonclassical Crystallization, *ACS Nano*, 2009, **3**, 1966–1978.
9 B. Xiang, D. J. Hwang, J. B. In, S. G. Ryu, J. H. Yoo, O. Dubon, A. M. Minor and C. P. Grigoropoulos, In Situ TEM Near-Field Optical Probing of Nanoscale Silicon Crystallization, *Nano Lett.*, 2012, **12**, 2524–2529.
10 J. Anwar and D. Zahn, Uncovering Molecular Processes in Crystal Nucleation and Growth by Using Molecular Simulation, *Angew. Chem., Int. Ed.*, 2011, **50**, 2–20.
11 M. Matsumoto, S. Saito and I. Ohmine, Molecular dynamics simulation of the ice nucleation and growth process leading to water freezing, *Nature*, 2002, **416**, 409–413.
12 F. H. Streitz, J. N. Glosli, M. V. Patel, B. Chan, R. K. Yates, B. R. Supinski, J. Sexton and J. A. Gunnels, Simulating Solidification in Metals at High Pressure: The Drive to Petascale Computing, *J. Phys.: Conf. Ser.*, 2006, **46**, 254–267.
13 X. D. Feng, D. C. Sayle, Z. L. Wang, M. S. Paras, B. Santora, A. C. Sutorik, T. X. T. Sayle, Y. Yang, Y. Ding, X. D. Wang and Y. S. Her, Converting ceria polyhedral nanoparticles into single-crystal nanospheres, *Science*, 2006, **312**, 1504–1508.
14 C. L. Freeman, J. H. Harding, D. Quigley and P. M. Rodger, Structural Control of Crystal Nuclei by an Eggshell Protein, *Angew. Chem., Int. Ed.*, 2010, **49**, 5135–5137.

15 K. Reed, A. Cormack, A. Kulkarni, D. Mayton, C. Sayle, F. Klaessig and B. Stadler, Exploring the Properties and Applications of Nanoceria: Is There Still Plenty of Room at the Bottom?, *Environ. Sci.: Nano*, 2014, **1**, 390–405.
16 A. Kumar, S. Das, P. Munusamy, W. T. Self, D. R. Baer, D. C. Sayle and S. Seal, Behavior of nanoceria in biologically-relevant environments, *Environ. Sci.: Nano*, 2014, **1**, 516–532.
17 T. X. T. Sayle, M. Cantoni, U. M. Bhatta, S. C. Parker, S. R. Hall, G. Moebus, M. Molinari, D. Reid, S. Seal and D. C. Sayle, Strain and Architecture-Tuned Reactivity in Ceria Nanostructures; Enhanced Catalytic Oxidation of CO to CO_2, *Chem. Mater.*, 2012, **24**, 1811–1821.
18 W. Smith and I. T. Todorov, A short description of DL_POLY, *Mol. Simul.*, 2006, **32**, 935–943.
19 D. C. Sayle, S. Seal, Z. W. Wang, B. C. Mangili, D. W. Price, A. S. Karakoti, S. V. T. N. Kuchibhatla, Q. Hao, G. Möbus, X. Xu and T. X. T. Sayle, Mapping Nanostructure: A Systematic Enumeration of Nanomaterials by Assembling Nanobuilding Blocks at Crystallographic Positions, *ACS Nano*, 2008, **2**, 1237–1251.
20 T. X. T. Sayle, P. E. Ngoepe and D. C. Sayle, *J. Mater. Chem.*, 2010, **20**, 10452–10458.
21 D. C. Sayle and T. X. T. Sayle, High-Pressure Crystallisation of TiO_2 Nanocrystals, *J. Comput. Theor. Nanosci.*, 2007, **4**, 299–308.
22 T. X. T. Sayle, C. R. A. Catlow, R. R. Maphanga, P. E. Ngoepe and D. C. Sayle, Modelling MnO_2 Nanoparticles using Simulated Amorphisation and Recrystallisation, *J. Am. Chem. Soc.*, 2005, **127**, 12828–12837.